Source deghosting for synchronized multi-level source streamer data

Zhan Fu, Nan Du, Hao Shen, Ping Wang, and Nicolas Chazalnoel (CGG)*

Summary

Ghost wavefield elimination is pivotal for improving the bandwidth and image resolution for marine seismic data. Synchronized multi-level source arrays, which aim to synchronize the primary wavefield and desynchronize the source ghost, will greatly attenuate the source ghost wavefield during acquistion. However, even with this advanced source design, some source deghosting is still needed and can be achieved using a 3D joint source inversion algorithm. We demonstrate that the joint source inversion method can properly and effectively eliminate the residual source ghost in the synchronized multi-level source streamer data using both 2D synthetic data and 3D real data examples.

Introduction

In marine seismic data, the primary limitation on frequency bandwidth comes from the notches generated by the interference between the primary and the free-surface ghost wavefields. To mitigate this limitation, variable-depth streamers (Soubaras, 2010, 2013) and synchronized multi-level source arrays (Siliqi et al., 2013) were introduced. Variable-depth streamers produce diversity in the receiver ghost notch that reduces notch effects and broadens the amplitude spectra of stacked images. Using a similar concept, synchronized multi-level source arrays are designed such that the down-going wavefields (primary) are synchronized, while the corresponding up-going wavefields (source ghosts) are desynchronized. Thus, the source ghost notches are attenuated during the acquisition. Zhou et al. (2014) demonstrated the benefits of combining these two acquisition technologies.

Even with these advanced acquisition techniques, appropriate deghosting methods are still required to producing ghost-free images. For example, several pre-migration deghosting algorithms (Riyanti et al., 2008; Wang et al., 2013, 2014; Poole, 2013) can be used to remove the receiver ghost energy for data with different streamer configurations as demonstrated by Hu et al. (2014). These receiver deghosting algorithms can also be used to approximate source deghosting by assuming a single point source, which is comparatively effective for single-level sources. For synchronized multi-level sources, one may naturally think deghosting is unnecessary because the source ghost wavefields are attenuated during acquisition. However, this is only partly true. We illustrate that residual ghost effects can still be observed in synchronized multi-level source streamer data. To effectively eliminate source ghost energy in the seismic data acquired with a modern complex air-gun array geometry, Wang et al. (2015) proposed an inversion scheme for 3D source deghosting that honors the air-gun array geometry. In this method, the synchronized primary from all sources was obtained by jointly inverting primary and ghosts for each of the sources in the Tau-P domain.

We applied the joint source inversion method to eliminate the source ghosts of synchronized multi-level sources on 2D synthetic data and on 3D field marine streamer data. In the synthetic data study, we validated the deghosting method for synchronized multi-level sources using the high similarity between the deghosted data and the modeled ghost-free data. In the field data study, we demonstrated the effectiveness and benefits of the source deghosting on pre-migration shot gathers, pre-stack depth migration (PSDM) images, and spectra.

The synchronized multi-level source

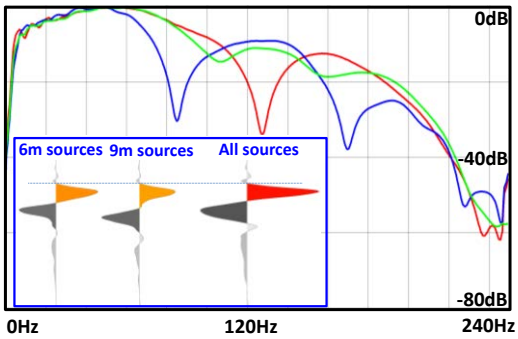

Figure 1: Source signature wavelets with their corresponding spectra for 6 m sources (red), 9 m sources (blue), and all sources (green).

To better understand the effect of multi-source arrays, we derived source signatures with their own ghosts from recorded near-field hydrophone (NFH) data (Ziolkowski et al., 1982). The whole source array was the combination of two level sources at 6 m and 9 m depth. Figure 1 shows three different vertical farfield signatures and their corresponding spectra: source signature from 6 m airguns, source signature from 9 m airguns, and source signature from the combined whole array. The two single-level-source signatures show source notches at expected frequencies according to their respective depths (125 Hz for the 6 m source; 83.3 Hz and 166.6 Hz for the 9 m source). The whole array signature did not contain an obvious notch at high frequency because of the natural cancellation of the

DOI http://dx.doi.org/10.1190/segam2015-5865771.1

ghost wavefields. However, all three wavelets still show a notch at low frequency at 0 Hz.

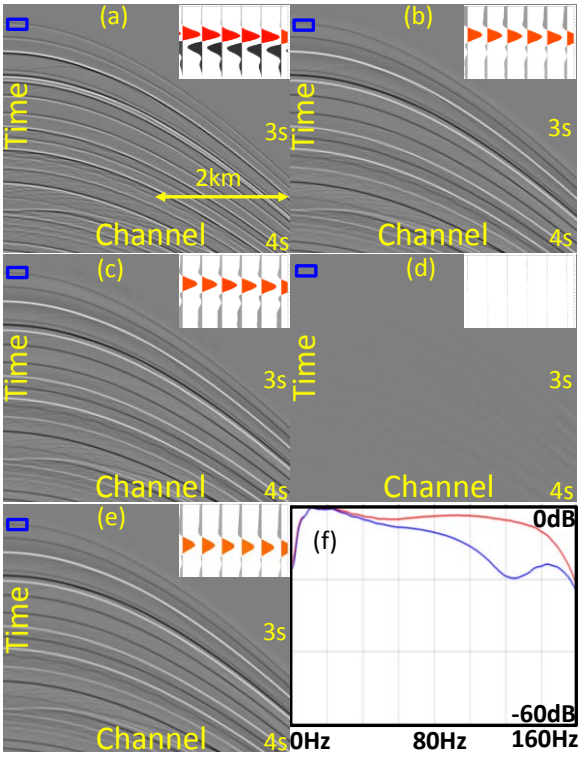

Figure 2: (a) A modeled shot using a modified Sigsbee2a model with source ghost, (b) modeled shot without source ghost, (c) deghosting output, (d) difference between (b) and (c), (e) source ghost with reversed polarity [difference between (b) and (a)], and (f) spectra of the modeled primary (red) and source ghost (blue). The wiggle views in (a)-(e) are zoom-ins of the blue boxes.

Both single-depth source wavelets have a strong trough (ghost) following the peak (primary), at about the same amplitude with time delays corresponding to the source depth (8 ms for the 6 m source; 12 ms for the 9 m source). The whole array wavelet also has a trough following the peak (primary). However, the trough has lower amplitude than the peak. This is because the ghost is already partially attenuated by the desynchronization during acquisition, and what we observe is the residual ghost.

The above analysis illustrates that residual ghosts still exist for the synchronized multi-level source. Moreover, even though the high-frequency ghost cancellation is well designed for an incident angle of 0 degrees, in practice it becomes less perfect as incident angle increases. As a result, high-frequency residual ghosts may be even stronger at far angles. Therefore, effort is still needed to eliminate the source ghost energies in the synchronized multi-level source data.

2D synthetic data study

We used a modified Sigsbee2a model to generate 2D synthetic data. To mimic the real data scenario, we placed sources at two levels (6 m and 9 m below the free surface) and synchronized them by firing them with a 2 ms time difference. The modeling did not contain receiver ghosts. Figures 2a-2c show the same modeled shot with ghost, without ghost (primary), and after deghosting, respectively. The ghost-free and deghosted shots are almost identical (their difference is shown in Figure 2d), which indicated that the joint source inversion algorithm is working properly. Figure 2e shows the difference between Figures 2a and 2b, which is the source ghost with reversed polarity. Contrary to a single-level source, where the ghost is just a delayed version of the primary with reverse polarity, in the synchronized multi-level source case the ghost does not look like the primary. The primary is also stronger than the ghost, particularly at high frequencies, as indicated by the spectra comparison (Figure 2f). Again, the amplitude difference between the primary and ghost is partly because the ghost energy has been cancelled by design during the acquisition. In real data, this lack of similarity could create some challenges when evaluating the deghosting result. Fortunately, in the joint source inversion algorithm, we can also output primary and ghost components for each source level. In this case, we expect a high level of similarity between the primaries and ghosts for each level of the sources—the summation of all components is equal to the input, and the summation of all primaries is equal to the deghosting output.

3D field data study

After evaluating the joint source inversion method for source deghosting on multi-level source synthetic data, we applied the algorithm to 3D field data acquired offshore Ivory Coast. The survey used synchronized multi-level sources and variable-depth streamer configurations. It covered a full fold area of more than 4300 km^2 in water depths ranging from 1700 m to 3700 m. Twelve solid streamers (8 km long) were towed at variable depths from 8 m (near channel) to 50 m (far channel). The receiver depths were optimized to provide the best notch diversity and receiver ghost cancellation for migration stacked images (Soubaras, 2010, 2013). The sources in this survey consisted of airguns at two different depths of 6 m and 9 m. The 9 m airguns were set to fire 2 ms after the 6 m airguns so that the deeper sources started when the down-going wavefields from the shallower sources reached them.

DOI http://dx.doi.org/10.1190/segam2015-5865771.1

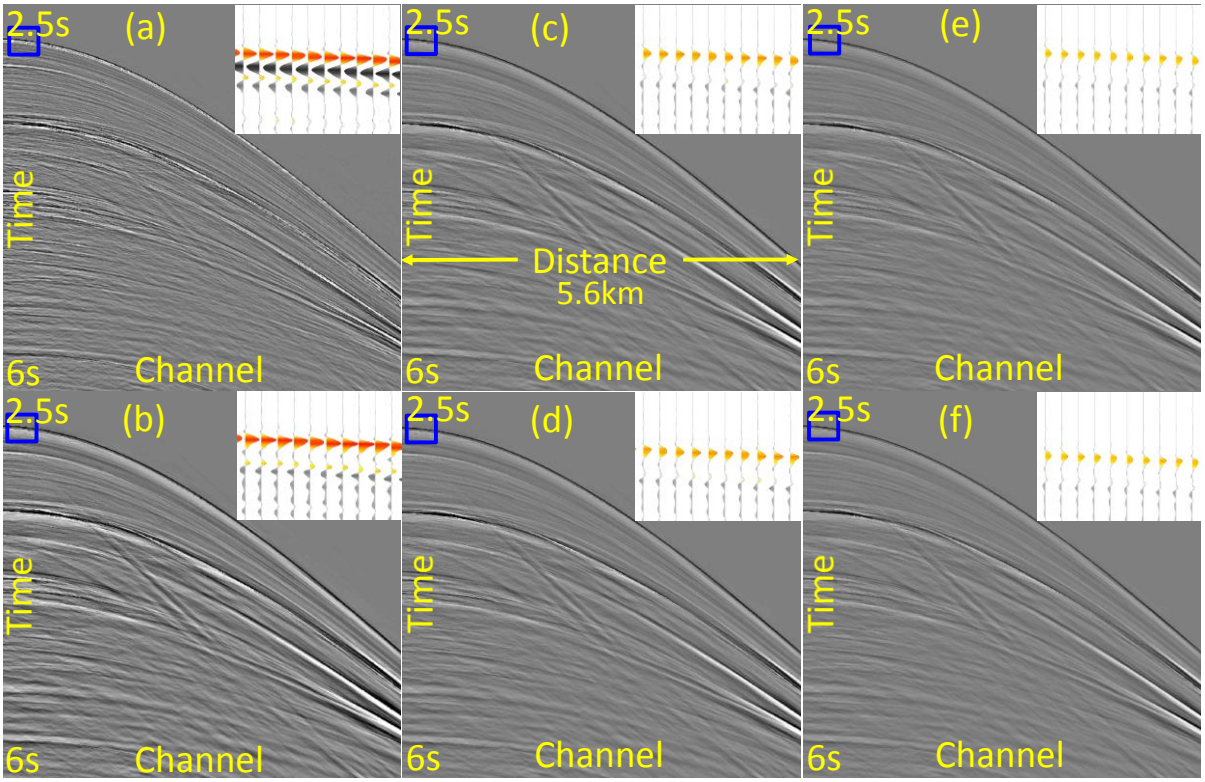

Figure 3: Shot gather of (a) source deghosting input, (b) source deghosting output, (c) 6 m primary, (d) 6 m ghost (reversed polarity), (e) 9 m primary, and (f) 9 m ghost (reversed polarity). The wiggle views are zoom-ins of the blue boxes in (a)-(f).

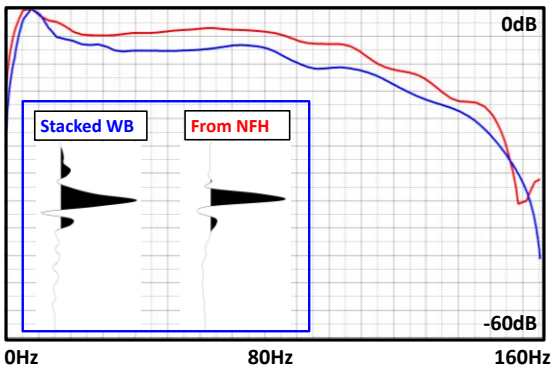

Figure 4: Amplitude spectra of ghost-free source signature derived from the near-field hydrophone (NFH) (red) and stacked water bottom wavelet after source deghosting (blue) along with the corresponding wavelets.

Input for the source deghosting was after sail line domain denoise, de-bubble, 3D receiver deghosting (Wang et al., 2014), zero-phasing, and 3D surface-related multiple elimination (SRME). Figure 3 shows a shot gather before and after the joint source inversion as well as all four components (6 m source primary and its ghost; 9 m source primary and its ghost). As expected, all four components look similar except for the starting time difference caused by the source depth difference and an amplitude difference relating to the source volume difference. The primary and ghost from the same source were almost identical with a slight time difference caused by different ray paths. We stacked the time aligned water bottom wavelet after source deghosting for the whole survey and compared it with the ghost-free source signature obtained from NFH recordings (Figure 4). The spectrum after deghosting was very close to that of the NFH ghost-free source wavelet. This indicated that the deghosting for both the source and receiver sides was accurate. At this stage, because the wavelet spectrum was not as flat as desired, a shaping filter could have been designed to tune the source wavelet and obtain a whiter spectrum as described by Poole et al. (2015).

Figures 5a-5d show stacked images and common image gathers (CIGs) from a 3D Kirchhoff PSDM of the data before and after source deghosting. Side lobes of events caused by ghosts were greatly attenuated in both the stack and CIG domain without introducing any artifacts, which greatly improved the interpretability of the image.

DOI http://dx.doi.org/10.1190/segam2015-5865771.1

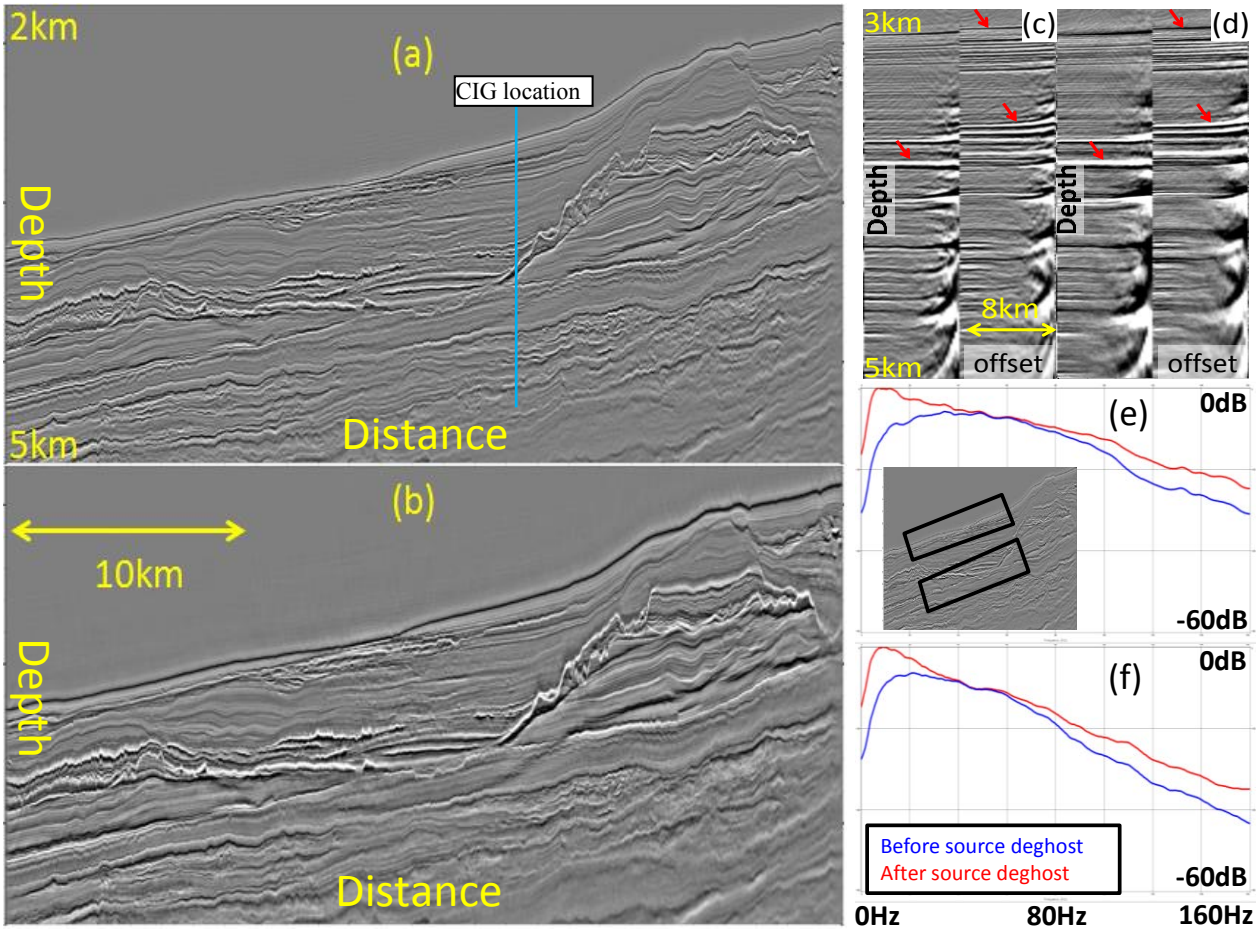

Figure 5: 3D Kirchhoff pre-stack depth migration (PSDM) image for the input data (a) before source deghosting and (b) after source deghosting, 3D Kirchhoff PSDM CIGs with input data (c) before source deghosting and (d) after source deghosting, and spectra measured from (e) a shallow window and (f) a deep window of the images in (a) (blue) and (b) (red). The two windows are indicated in (e).

Spectra relating to the different windows in Figures 5e and 5f confirmed the effective spectrum expansion from the source deghosting. Due to dispersion and absorption effects, the deeper window spectrum exhibited high-frequency amplitude decay. We expect that background amplitude Q compensation (Zhou et al., 2014) or post-migration bandwidth extension (C. Peng, personal communication, 2015) could further extend the high frequency in the deeper window and improve the image quality.

Conclusions

This study demonstrated that residual source ghosts still exist in marine data even from a 3D synchronized multi-level source acquisition. These residual ghosts can be effectively removed by the joint source inversion algorithm. As a result, the amplitude spectrum was extended to both low and high frequencies, which improved the resolution and interpretability of the seismic image and paved the way to fully using the potential of broadband acquisition. To fully utilize the source array information, in future studies we will apply 3D directional designature (Poole et al., 2015, Wang et al., 2015), which will compensate source directivity compared with the 1D zero-phasing filter we used in this study.

Acknowledgments

The authors thank CGG for the permission to present the data and publish the work.

DOI http://dx.doi.org/10.1190/segam2015-5865771.1

EDITED REFERENCES

Note: This reference list is a copyedited version of the reference list submitted by the author. Reference lists for the 2015 SEG Technical Program Expanded Abstracts have been copyedited so that references provided with the online metadata for each paper will achieve a high degree of linking to cited sources that appear on the Web.

REFERENCES

Hu, B., H. Shen, P. Wang, and V. Tyagi, 2014, Premigration ghost wavefield elimination on different cable configurations: A case study in the Gulf of Mexico: 76th Conference & Exhibition, EAGE, Extended Abstracts, http://dx.doi.org/10.3997/2214-4609.20140699.

Poole, G., 2013, Pre-migration receiver de-ghosting and re-datuming for variable depth streamer data: 83rd Annual International Meeting, SEG, Expanded Abstracts, 4216–4220.

Poole, G., J. Cooper, S. King, and P. Wang, 2015, 3D source designature using source-receiver symmetry in the shot tau-px-py domain: 77th Conference & Exhibition, EAGE, Extended Abstracts, doi:10.3997/2214-4609.201413193.

Riyanti, C. D., R. G. van Borselen, P. M. van den Bert, and J. T. Fokkema, 2008, Pressure wave-field deghosting for non-horizontal streamers: 78th Annual International Meeting, SEG, Expanded Abstracts, 2652–2656.

Siliqi, R., T. Payen, R. Sablon, and K. Desrues, 2013, Synchronized multi-level source — A robust broadband marine solution: 83rd Annual International Meeting, SEG, Expanded Abstracts, 56–60.

Soubaras, R., 2010, Deghosting by joint deconvolution of a migration and a mirror migration: 80th Annual International Meeting, SEG, Expanded Abstracts, 3406–3410.

Soubaras, R., 2013, Optimization of the streamer shape in variable-depth streamer acquisitions: 75th Conference & Exhibition, EAGE, Extended Abstracts, doi:10.3997/2214-4609.20130490.

Wang, P., K. Nimsaila, D. Zhuang, Z. Fu, H. Shen, G. Poole, and N. Chazalnoel, 2015, Joint 3D source-side deghosting and designature for modern air-gun arrays: 77th Conference & Exhibition, EAGE, Extended Abstracts, doi:10.3997/2214-4609.201413190.

Wang, P., S. Ray, and K. Nimsaila, 2014, 3D joint deghost and crossline interpolation for marine single-component streamer data: 84th Annual International Meeting, SEG, Expanded Abstracts, 3594–3598.

Wang, P., S. Ray, C. Peng, Y. Li, and G. Poole, 2013, Premigration deghosting for marine streamer data using a bootstrap approach in tau-p domain: 83rd Annual International Meeting, SEG, Expanded Abstracts, 4221–4225.

Zhou, J., J. Li, H. Ng, S. Birdus, T. K. Huat, P. Y. Peng, J. Sun, H. Yi, and P. Chia, 2014, Unlocking the full potential of broadband data with advanced processing and image technology — A case study from NWS Australia: 84th Annual International Meeting, SEG, Expanded Abstracts, 3689–3693.

Ziolkowski, A., G. E. Parkes, L. Hatton, and T. Haugland, 1982, The signature of an air gun array: Computation from near-field measurements including interactions: Geophysics, **47**, 1413–1421, http://dx.doi.org/10.1190/1.1441289.

DOI http://dx.doi.org/10.1190/segam2015-5865771.1